A novel approach to sustain Fe^0-electrocoagulation for Cr(VI) removal by optimizing chloride ions

Hai-yin Xu [a,b], Zhao-hui Yang [a,b,*], Yuan-ling Luo [c], Guang-ming Zeng [a,b], Jing Huang [a,b], Li-ke Wang [a,b], Pei-pei Song [a,b], Xia Yang [a,b]

[a] College of Environmental Science and Engineering, Hunan University, Changsha 410082, PR China
[b] Key Laboratory of Environmental Biology and Pollution Control (Hunan University), Ministry of Education, Changsha 410082, PR China
[c] Changsha Environmental Protection College, Changsha 410004, PR China

ARTICLE INFO

ABSTRACT

Chloride (Cl$^-$) is widely used for depassivation in electrocoagulation using metallic iron (Fe^0-EC). However, its optimization is still on a pragmatic approach and thus of limited success. This study proposed a novel approach based on a systematic investigation of Cl$^-$–induced pitting dissolution behavior of Fe^0 with the evolution of pH and Cr(VI) ($0 \leqslant$ Cr(VI) (mg/L) $\leqslant 520$) in Fe^0-EC. The depassivation behavior was characterized by potentiodynamic polarization, cyclic voltammograms (CVs), galvanostatic measurements, and scanning electron microscope (SEM) analysis. The proposed approach to optimize Cl$^-$ for depassivation was as follows: (1) Build a database of minimum Cl$^-$ concentrations for pitting dissolution (MCPD) as a function of pH and Cr(VI) in passivation region III (MCD = f(pH, Cr(VI))); (2) Record the curve function (g) of pH and Cr(VI) evolution ($g = \{(pH_i, Cr(VI)_i), \ldots, (pH_f, Cr(VI)_f)\}$) without passivation in the Fe^0-EC process; (3) Obtain the optimal concentration of Cl$^-$ for depassivation (OCD) by selecting the maximum MCDs by combining the curve (g) and the database of MCPD (OCD = $Max\{MCPD_1, MCPD_2, \ldots MCPD_n\}$). This method was more accurate and stable compared with RSM.

© 2015 Elsevier B.V. All rights reserved.

1. Introduction

Electrocoagulation (EC) is an attractive technology for Cr(VI) removal because of its advantages of in-situ Fe(II)-coagulant production [1–5], by-product (H$_2$) recovery [6,7], and high automation level [8–10]. In particular, Fe^0-EC has been applied to decrease Cr(VI) discharges to the Xiangjiang River as part of the "12th Five-year Plan" to prevent heavy metal pollution in the Hunan Province [9].

However, the passivation is widely observed in the Fe^0-EC process for Cr(VI) removal [8,9,11,12]. It severely limits the widespread application of EC because it decreases the Cr(VI) removal efficiency [8,12], induces higher power consumption [13], and restricts hydrogen recovery [7,11]. Thus, the effective methods of arresting passivation in the Fe^0-EC process are urgently required.

Reported methods for depassivation include the mechanical cleaning [14], alternating pulsed current (APC) [12,15,16] and introducing aggressive agent [8,9,11,16–20]. In practice, the strategy by introducing aggressive agent, especially Cl$^-$, is an effective and widely used method for depassivation in the large-scale and continuous Fe^0-EC processes for Cr(VI) removal [8,9,11]. It has to be mention that insufficient Cl$^-$ is unable to avoid passivation [8], conversely, the excess one will restrict the reuse of treated water [21].

The optimal concentration of Cl$^-$ for depassivation is the one that just prevents the occurrence of passivation in the EC process. The approach to optimize Cl$^-$ for depassivation of Fe^0-EC is still very limited and only restricted to the response surface methodology (RSM) with current efficiency (CE) as response value [19]. However, RSM has strict requirements on selection of the influencing factor's range. Additionally, the calculation of CE is a time-consuming process due to the determination step of total dissolved iron [12].

So is there any other time-saving way to optimize the content of Cl$^-$ for depassivation in the Fe^0-EC process for Cr(VI) removal? To answer this question, we first need to know what and how to influence the resistance of Cl$^-$ for depassivation in Fe^0-EC process, however, the crucial knowledge about it is still lacking.

In corrosion field, the behavior of Cl$^-$ for depassivation has been largely investigated in the Fe^0/H$_2$O system, a similar system as

* Corresponding author at: College of Environmental Science and Engineering, Hunan University, Changsha 410082, PR China.
 E-mail address: yzh@hnu.edu.cn (Z.-h. Yang).

Fe⁰-EC [22,23]. The depassivation process is due to the fact that Cl⁻ covering passive oxide film promotes selective dissolution of iron hydroxide/oxide precipitation as soluble FeCl$_2$ and FeCl$_3$ in the vicinity of metals [24–26]. The resistance of Cl⁻ for depassivation is relative to the solution pH [24–27], inhibitors (such as CrO$_4^{2-}$, MoO$_4^{2-}$, and WO$_4^{2-}$) [28,29] and composition and construction of passive film [30,31]. Specially, the corrosion risk of mild steel associated to a certain Cl⁻ content is usually evaluated in terms of the [Cl⁻]/[OH⁻] ratio [26]. CrO$_4^{2-}$ anion increases the protectiveness of passive film not only by its higher specific adsorption than Cl⁻ [28] but also by its role in promoting passive film formation [12,29]. The Cl⁻-induced pitting resistance is improved by forming a protective barrier film with an enrichment of chromium oxide [30].

The Fe⁰-EC system can be essentially considered as an electrochemically ($U_0 \neq 0$) driven accelerated corrosion process [22,23]. However, the resistance of Cl⁻ for depassivation in Fe⁰-EC is more complicated than that in Fe⁰/H$_2$O system. In Fe⁰-EC system, the evolution of pH and Cr(VI) varies with the increasing treatment time, and thereby influences the behavior of passivation/depassivation by changing the relative kinetics of dissolution and precipitation [9,12]. Additionally, the composition of passive films is highly depended on pH and Cr(VI) concentration [12]. So, the optimum of Cl⁻ content is changing all the time due to the variation of pH and Cr(VI) and passive film composition in Fe⁰-EC process. Therefore the optimal concentration of Cl⁻ for depassivation is making the passivation not occur with the evolution of pH and Cr(VI) in Fe⁰-EC process.

Above all, firstly, we needed to study the effects of the evolution of pH with Cr(VI) removal on passivation in Fe⁰-EC process. Secondly, the influence of pH and Cr(VI) on chloride-induced pitting dissolution should be investigated. And then, the content of Cl⁻ for Fe⁰-EC depassivation was optimized in conjunction with the evolution of pH and Cr(VI) by the above proposed method and finally compared with RSM.

2. Material and methods

2.1. Electrocoagulation experiments

2.1.1. Experimental set-up
The electrocoagulation set-up consisted of a 2.5 L reactor with two iron rod (99.5% Fe) electrodes of 20 cm^2 active surface area and 25 mm inter-electrode spacing. The electrodes, polished by 800 grit SiC papers, were connected to a programmable DC power supply (RIGOL DP1116A, China) with a constant current density 100 A m^{-2}. Synthetic solutions containing Cr(VI) and Cl⁻ were prepared with appropriate amount of K$_2$Cr$_2$O$_7$ and NaCl into distilled water respectively to yield varying concentrations. And the K$_2$SO$_4$ was used as the supplementary supporting electrolyte to maintain the electrical conductivity. The solution pH was adjusted by adding 0.5 M NaOH or H$_2$SO$_4$ solutions and measured by pH meter (FE20, METTLER TOLEDO, Switzerland). A faster stirring rate of 600 rpm was used during the experiments [16]. A first set of samples (15 mL) was filtered through 0.45 μm nylon filters for the determination of Cr(VI) [32]. A second set of unfiltered samples (15 mL) was taken and digested in HNO$_3$ before analysis for the determination of Fe(Tot) [32]. All experiments were conducted at room temperature (23 ± 2 °C).

2.1.2. RSM experimental design
The central composite design (CCD), a standard RSM, was selected to verify the results of the factors (initial pH (x_{i1}) and Cl⁻ (x_{i2})) on the CE (y_i) at Cr(VI) concentration 104, 260 and 520 mg L^{-1} respectively. All factors were controlled at five levels.

The response variable (y_i) that represented CE was fitted by a second-order model in the form of quadratic polynomial equation:

$$y = \beta_0 + \sum_{i=1}^{m} \beta_i x_i + \sum_{i<j}^{m} \beta_{ij} x_i x_j + \sum_{i=1}^{m} \beta_{ii} x_i^2 \tag{1}$$

where y is the response variable to be modeled. x_i and x_j are independent variables which determine y. β_0, β_i and β_{ii} are the offset term, the linear coefficient and the quadratic coefficient, respectively. β_{ij} is the term that reflect the interaction between x_i and x_j. The actual design ran by the statistic software, Design-expert 7.1.3 (Stat-Ease Inc, USA), is presented in Table 1.

2.1.3. Calculation of current efficiency (CE)
The CE was calculated using the following equations:

$$CE = \frac{\Delta m_{exp}}{\Delta m_{theo}} = \frac{Fe(Tot) \cdot V \cdot n \cdot F}{0.1 \cdot M \cdot i \cdot A \cdot t} \cdot 100\% \tag{2}$$

where Δm_{exp} is the actual dissolved iron (g), Δm_{theo} is the theoretical dissolved iron (g), Fe(Tot) is the concentration of dissolved iron (mg L^{-1}), V is the volume of wastewater (L), t is the time of electrolysis (s), M is the atomic weight of the iron (56 g mol^{-1}), i is the current density (A m^{-2}), A is the surface area of anode (cm^2), n is the number of electron moles ($n = 2$) and F is the Faraday's constant (96,487 C mol^{-1}).

2.2. Electrochemical experiments

2.2.1. Electrochemical cell and electrode preparation
Electrochemical measurements were conducted on the electrochemical work station (CHI 760E, china) with a standard three-electrode cell. The working electrode, a pure iron disc (99.9%), was embedded in resin with an exposed area of 8.3 mm^2. A large-area platinum electrode was used as counter electrode and a Hg/Hg$_2$SO$_4$ (saturated K$_2$SO$_4$) reference electrode as the reference electrode, which was connected to the cell by a luggin capillary as described previously [12]. The working surface ground with 800 grit SiC papers, followed by a wet finish (0.3 μm alumina), and sonicated in an ethanol for 5 min. Solutions were deaerated by N$_2$ for 30 min before use. All potentials were quoted on the Hg/Hg$_2$SO$_4$ scale (0.418 V vs. SCE, 0.659 V vs. SHE).

2.2.2. Chronopotentiometry
The passive films was obtained by the chronopotentiometry with the identical operational parameters (current density, reaction time, and stirring rate) as that in Fe⁰-EC reactor and then used for further analysis by potentiodynamic polarization, cyclic voltammograms and galvanostatic measurement.

2.2.3. Potentiodynamic polarization
Potentiodynamic polarization experiments were carried out in pH 8 and Cr(VI) = 260 mg L^{-1} solution with different concentration of Cl⁻ (0, 17, 18 and 19 mM). The scan rate was 1 mV s^{-1} and the

Table 1
Coded levels of 2 variables framed by CCD.

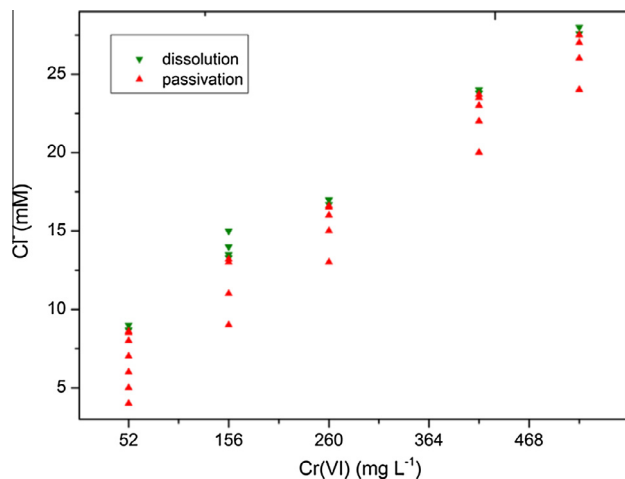| Cr(VI) (mg L^{-1})	Factors	Codes	Coded levels				
			−1.414	−1	0	+1	+1.414
104	Initial pH	x_{11}	2.70	3.33	4.85	6.37	7.00
	Cl⁻	x_{12}	0	1.76	6.00	10.24	12.00
260	Initial pH	x_{21}	2.30	2.99	4.65	6.31	7.00
	Cl⁻	x_{22}	0	2.20	7.50	12.80	15.00
520	Initial pH	x_{31}	2.00	2.73	4.50	6.27	7.00
	Cl⁻	x_{32}	5.00	7.93	15.00	22.07	25.00

Fig. 1. Schematic illustration of determining the minimum Cl^- for pitting dissolution by galvanostatic measurements in pH 8 with different Cr(VI) concentrations (52, 156, 260, 416 and 520 mg L^{-1}).
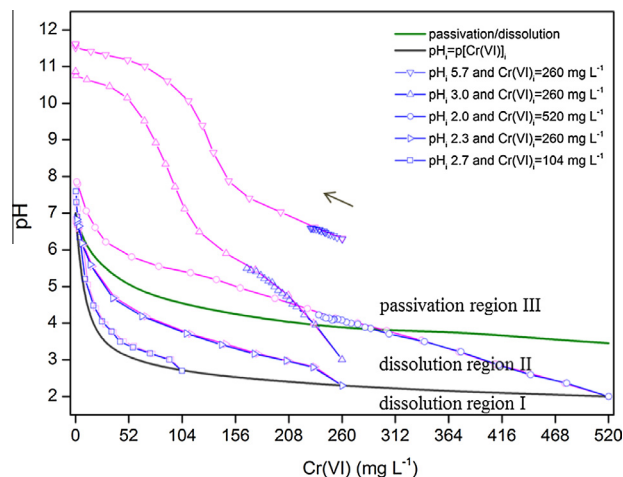

Fig. 2. Evolution of pH and Cr(VI) concentration at regular intervals (5 min) during Fe^0-EC process corresponding to different initial pH and Cr(VI) concentrations. The pink line is with 15 mM Cl^- addition, whereas the blue line without Cl^- addition. The green line is the boundary of passivation and depassivation, and the black line is acidic and alkaline of final pH. (For interpretation of the references to color in this figure legend, the reader is referred to the web version of this article.)

starting potential was −150 mV versus open-circuit potential. The test was terminated when the current density exceeded 2.0 A m^{-2}.

2.2.4. Cyclic voltammograms (CVs)

The CVs were used to evaluate the electrochemical characterization of the treated samples by chronopotentiometry in different pH_i-$Cr(VI)_i$ before and after Cl^- (12 mM) addition at a sweep rate of 10 mV s^{-1}.

2.2.5. Galvanostatic measurements

Galvanostatic measurements were performed to determine the behavior of passivation or depassivation as described previously [12]. A constant current of 8.3E-4 A (ca. 100 A m^{-2}) was applied during each experiment and the potential was recorded as a function of time. The criterion of passivation/depassivation were as follows: the electrode potential value, above the reversible potential of oxygen evolution indicated the occurrence of passivation, otherwise, the potential between the reversible potential of oxygen evolution and hydrogen evolution indicated the depassivation or pitting dissolution of iron. Then the minimum Cl^- for pitting dissolution (MCPD) of treated samples were determined by the above criterion with different pH and Cr(VI), as shown in Fig. 1.

2.2.6. Scanning electron microscope (SEM)

Morphological observations of iron electrode surfaces of CVs and EC process with Cl^- (12 mM) addition were achieved by SEM (Quanta 200 FEG, FEI, US).

3. Results and discussion

3.1. Effects of pH and Cr(VI) evolution on passivation of Fe^0-EC

A pH–Cr(VI)-dissolution/passivation diagram, as described previously [12], was constructed using the dissolution (I, II) and passivation regions (III) shown in Fig. 2. Passivation inevitably occurs if the evolution of pH and Cr(VI) is in the passivation region III of Fe^0-EC [12]. The dissolution region was divided into dissolution region I and dissolution region II depending on the relative magnitude of chromic alkalinity (p[Cr(VI)]) and initial pH (pH_i) of Fe^0-EC. Specifically, dissolution I, the region of p[Cr(VI)] > pH_i, achieved an acidic final pH and low removal efficiency of Cr(III), while dissolution II, the region of p[Cr(VI)] ⩽ pH_i, achieved a reasonable final pH for

Cr(III) precipitation and did not suffer passivation, which was optimal condition for EC operation [9].

The evolution of pH and Cr(VI) was a continuous process as Cr (VI) was removed during the Fe^0-EC process [12,16]. So, a transition from the dissolution to passivation region may occur during the evolution of pH and Cr(VI), which relies heavily on the respective initial values of pH and Cr(VI) [9].

For pH_i 2.7 and $Cr(VI)_i$ = 104 mg L^{-1}, irrespective of the addition of Cl^- (Fig. 2), the evolution of pH and Cr(VI) featured the same with treatment time and were invariably located in dissolution region II until Cr(VI) was removed completely, which implies that passivation did not occur throughout. Similar behavior was also observed in pH_i 2.3 and $Cr(VI)_i$ = 260 mg L^{-1}.

In contrast, for pH_i 2.0 and $Cr(VI)_i$ = 520 mg L^{-1} with Cl^-, the evolution of pH and Cr(VI) crossed sequentially from dissolution region II to passivation region III during the removal of Cr(VI). There were similar variations of pH and Cr(VI) in dissolution region II without Cl^-, but their evolution was interrupted when entering the passivation region III. This was due to passivation hindering the removal of Cr(VI) by forming a passive oxide film [12]. Similar evolution was observed in pH_i 3 and $Cr(VI)_i$ = 260 mg L^{-1} and pH_i 5.7 and $Cr(VI)_i$ = 260 mg L^{-1}.

Based on the above results, it could be conclude that passivation is related to the initial values of pH and Cr(VI) and their evolution. Concretely, passivation inevitably occurs when pH_i and $Cr(VI)_i$ are in passivation region III or the evolution of pH and Cr(VI) enter passivation region III, even if their initial values are in dissolution region II. Additionally, the passivation region occupies the majority of the pH–Cr(VI) diagram, thus it is necessary to investigate the quantitative influence of pH and Cr(VI) on chloride-induced pitting dissolution and optimize concentration of Cl^- in the depassivation of Fe^0-EC.

3.2. Minimum chloride for pitting dissolution (MCPD) of Fe^0-EC

3.2.1. Effects of chloride on pitting dissolution

The effects of different concentrations of Cl^- on pitting dissolution were investigated through potentiodynamic polarization experiments (Fig. 3). The region between 0.15 and 0.75 V (vs. Hg/Hg$_2$SO$_4$), which had a roughly constant current density, was regarded as the classic passivation region [31]. A small current density (<0.1 A m^{-2}) was observed in this region both with and
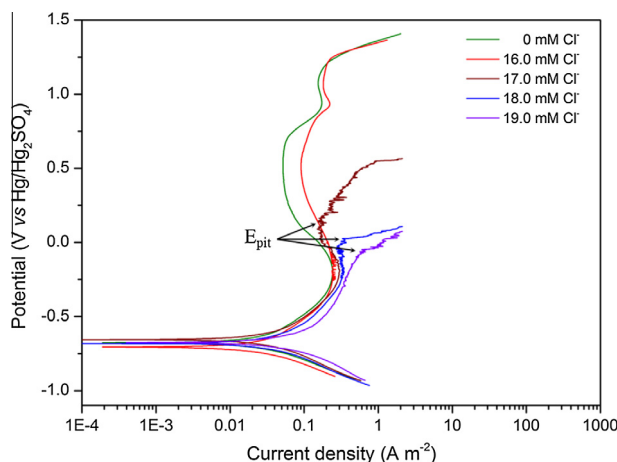
Fig. 3. Potentiodynamic polarization curves: the effects of different Cl$^-$ concentrations on pitting dissolution in pH 8 and Cr(VI) = 260 mg L^{-1}.

without the addition of a concentration of 16.0 mM Cl$^-$, which indicated that the dissolution of iron was significantly suppressed in the passivation region by the passive film that formed [24,26].

With increased concentrations of 17.0, 18.0 and 19.0 mM of Cl$^-$, the pitting dissolution phenomenon occurred along with a series of current transients followed by a rapid rise in current [33]. This was due to the breakdown of passive film by the Cl$^-$covering, which

promotes the selective dissolution of passive films as soluble Fe (Cl)$_n$ in the vicinity of an anode and then avoids iron hydroxide/ oxide precipitation [34,35]. Notably, pitting potential (E_{pit}), as a pitting susceptibility indicator, became more negative as Cl$^-$ increased [26,36]. It is also reasonable to assume that there is an optimal concentration of Cl$^-$ to induce pitting dissolution for both pH and Cr(VI) in passivation region III.

3.2.2. Effects of pH and Cr(VI) on chloride-induced pitting dissolution

The effects of pH and Cr(VI) on chloride-induced pitting dissolution were examined through CVs and surface analyses (Fig. 4). Identical CVs (Fig. 4a) and smooth surfaces without pitting (Fig. 4b and c) both with and without Cl$^-$ were observed. The anode remained in the passivation region with the addition of a concentration of 12.0 mM Cl$^-$ in pH 8 and Cr(VI) = 520 mg L^{-1}[28]. As pH (pH 4 and Cr(VI) = 520 mg L^{-1} with 12 mM Cl$^-$) decreased, the growth of metastable pits was initiated by typical transient current density and the decay of current density (Fig. 4d) with a limited number of pits on the surface of the anode (Fig. 4e and f). This observation can be interpreted by the relative kinetics of the iron dissolution process (v_d) and its precipitation process (v_p), which occurs in the process of Fe^0-EC [12]. In particular, a sudden increase in current density indicated pitting dissolution since the anion diffuse layer of OH$^-$ promoted iron hydroxide/oxide precipitation, which led to $v_d > v_p$[3,24]. The ensuing decay of current density was due to chromate-induced repassivation. Chromate forms a passive film by displacing the absorbed Cl$^-$ and
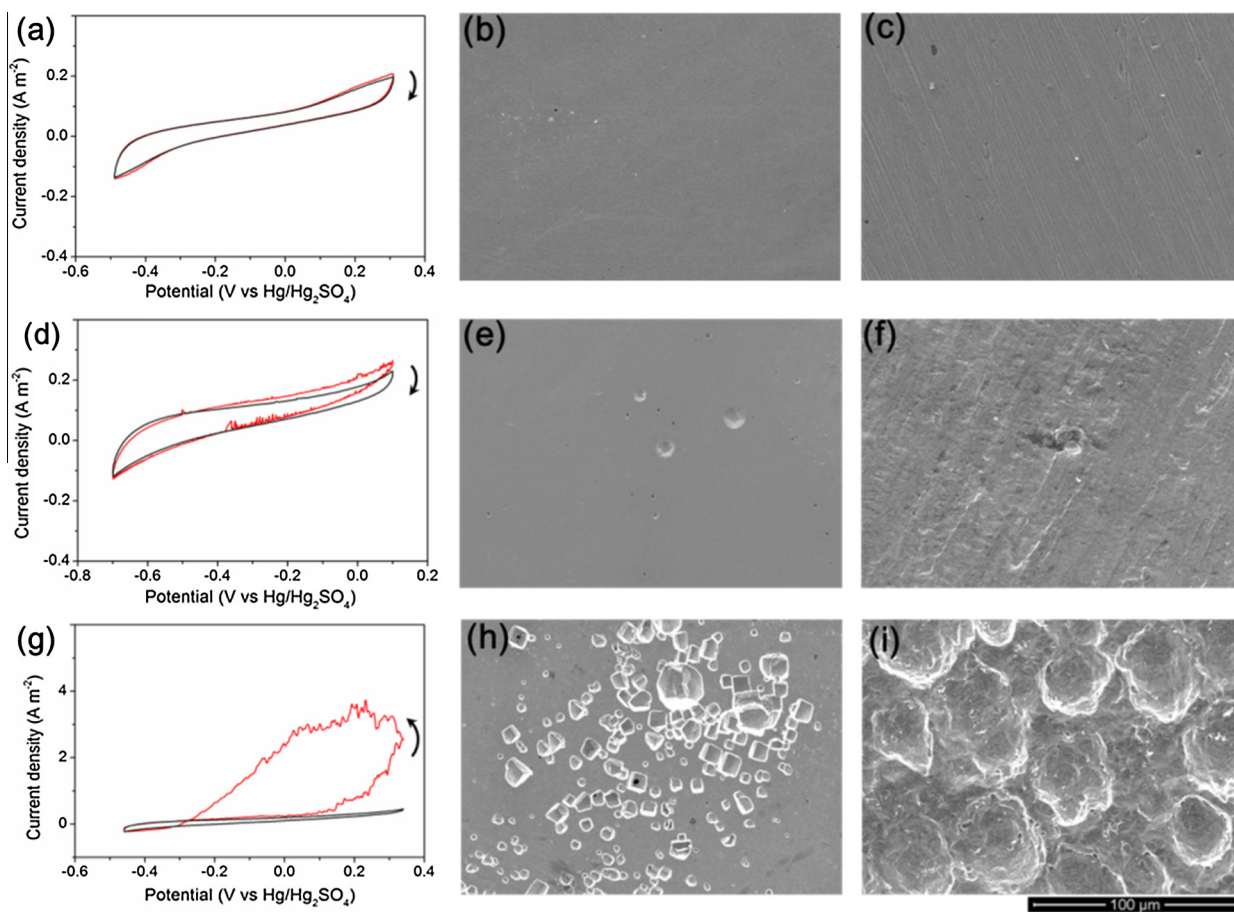

Fig. 4. Comparison of CVs. and SEM images at pH 8 and Cr(VI) = 520 mg L^{-1} (a–c), pH 4 and Cr(VI) = 520 mg L^{-1} (d–f), and pH 8 and Cr(VI) = 52 mg L^{-1} (g–i). The CVs. (a, d, and g) were recorded on the respective solutions before (dark line) and after (red line) Cl$^-$ addition (12 mM). The SEM images of CVs. (b, e, and h) and Fe^0-EC (c, f, and i) were then obtained with Cl$^-$ addition (12 mM). (For interpretation of the references to color in this figure legend, the reader is referred to the web version of this article.)

consequently causing $v_d < v_p$, which increases the protectiveness of the passive film [12,29].

It should be noted that there is a rapid increase in current densities for potentials >0.92 V *vs.* Hg/Hg$_2$SO$_4$ with sweep time increasing in pH 8 and Cr(VI) = 52 mg L^{-1} (Fig. 4g). Actually, the current density of the potential sweep moving toward the negative was higher than the previous potential sweep moving toward the negative because of changes to the surface area. A larger surface area was created by the incorporative pits, which gradually merged with the larger ones with potential sweep (Fig. 4h and i) [37]. Therefore, the sequence of the resistance of chloride-induced pitting dissolution in these three conditions is pH 8 and Cr(VI) = 520 mg L^{-1} > pH 4 and Cr(VI) = 520 mg L^{-1} > pH 8 and Cr(VI) = 52 mg L^{-1}, which is consistent with the stability of its passive film [12].

3.2.3. Database of MCPD in passivation region (III)

As previously discussed, the resistance of chloride-induced pitting dissolution decreased as the concentration of Cl$^-$ increased and increased as pH and Cr(VI) increased, which is consistent with the stability of its passive film. Therefore, there must be an MCPD for both pH and Cr(VI) in passivation region III. It was determined from galvanostatic measurements, as shown in Fig. 5.

3.3. Optimum chloride for depassivation (OCD) in Fe^0-EC process

Based on the results presented in the preceding sections, the optimal concentration of Cl$^-$ for depassivation is that which prevents passivation during the evolution of pH and Cr(VI) in the Fe^0-EC process. The proposed approach to optimize Cl$^-$ for depassivation is as follows:

(1) Build a database of minimum Cl$^-$ concentrations for pitting dissolution (MCPD) as a function of pH and Cr(VI) in passivation region III (MCD = f (pH, Cr(VI))).
(2) Record the curve function (g) of pH and Cr(VI) evolution (g = {(pH$_i$, Cr(VI)$_i$), ..., (pH$_f$, Cr(VI)$_f$)}) without passivation in the Fe^0-EC process.
(3) Obtain the optimal concentration of Cl$^-$ for depassivation (OCD) by selecting the maximum MCDs by combining the curve (g) and the database of MCPD (OCD = Max\{MCPD$_1$, MCPD$_2$, ... MCPD$_n$\}).

Take pH$_i$ 6.31 and Cr(VI)$_i$ = 260 mg L^{-1} for example. First, a database of minimum Cl$^-$ concentrations for pitting dissolution
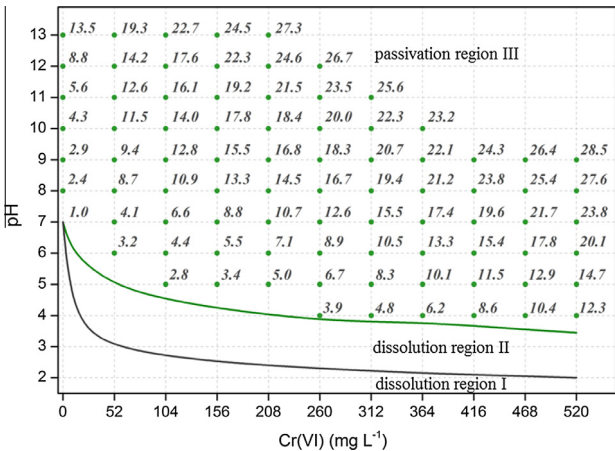
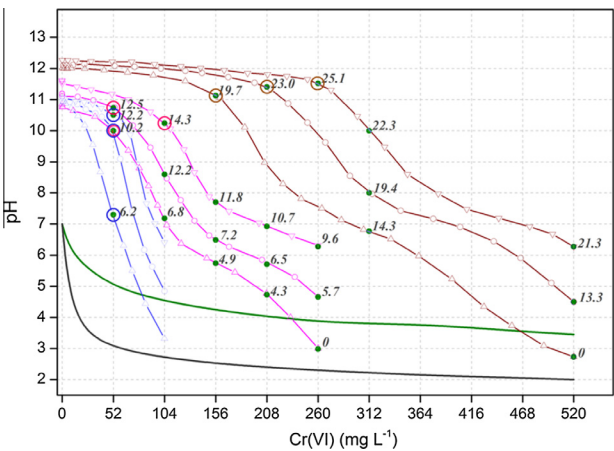**Fig. 5.** Database of MCPD corresponding to pH and Cr(VI) in the passivation region III.

Fig. 6. Evolution of pH and Cr(VI) and corresponding optimization of Cl$^-$ for depassivation for Cr(VI)$_i$ = 104 mg L^{-1}, pH$_i$ = 3.30, 4.85, and 6.37; Cr(VI)$_i$ = 260 - mg L^{-1}, pH$_i$ = 3.0, 4.65, and 6.31; and Cr(VI)$_i$ = 520 mg L^{-1}, pH$_i$ = 2.73, 4.50, and 6.27 in Fe^0-EC process.

(MCPD) as a function of both pH and Cr(VI) in passivation region III (MCD = f (pH, Cr(VI))) was built. This database is described in Section 3.2.3. Following this, the curve function of pH and Cr(VI) evolution (g = {(6.31, 260), ..., (pH$_f$, Cr(VI)$_f$)} without passivation (30 mM Cl$^-$) was recorded (Fig. 6). Finally, the optimal concentration of Cl$^-$ for depassivation (OCD) was obtained by selecting the maximum MCDs by combining the curve (g) and the database of MCPD (OCD = Max\{MCPD$_1$, MCPD$_2$, ... MCPD$_n$\} = Max (9.6, 10.7, 11.8, 14.3) = 14.3).

The same steps were used to optimize for other conditions. These results are shown in Table 2. A high CE (from 97.2% to 99.7%) was also obtained from validation experiments, of which the relative error was less than 2.2%. Next, RSM was used to further confirm the accuracy of our proposed method.

3.4. Verification using RSM

The central composite design of RSM was developed to obtain the optimal concentration of Cl$^-$ for depassivation in the Fe^0-EC process. Table 3 shows the experimental matrices for two variables (initial pH (x_{i1}) and Cl$^-$ (x_{i2})) and corresponding experimental responses (CE (y_i)) for three concentrations of Cr(VI) (104, 260 and 520 mg L^{-1}). The discrepancies (ANOVA) of RSM models were analyzed based on the results in Table 3. The results revealed that three models are highly significant (i.e., "Prob > F" < 0.0001, <0.0001 and 0.0001 for 104, 260 and 520 mg L^{-1}, respectively) with an insignificant *lack of fit* ("Prob > F" 0.1135, 0.0545 and 0.0535 for 104, 260 and 520 mg L^{-1}, respectively). This conclusion

Table 2
Optimal Cl$^-$ for depassivation in Fe^0-EC by proposed method.

Concentration (mg L^{-1})	Initial pH	Optimal Cl$^-$ (mM)	CE (%)		Relative Error (%)
			Prediction	Validation	
260	3.00	10.2	100	99.7	0.3
104	3.30	6.2	100	97.8	2.2
	4.85	10.2	100	99.2	0.8
	6.37	12.2	100	98.6	1.4
260	3.00	10.2	100	99.7	0.3
	4.65	12.5	100	99.5	0.5
	6.31	14.3	100	99.3	0.7
520	2.73	19.7	100	98.5	1.5
	4.50	23.0	100	97.2	2.9
	6.27	25.1	100	99.6	0.4

Table 3
Experimental matrix for the variables and corresponding experimental response.

Run	104 mg L^{-1}				260 mg L^{-1}				520 mg L^{-1}			
	Std	x_{11}	x_{12} (mM)	y_1 (%)	Std	x_{21}	x_{22} (mM)	y_2 (%)	Std	x_{31}	x_{32} (mM)	y_3 (%)
1	3	3.33	10.24	103.1	6	7.00	7.50	33.2	8	4.50	25.00	98.7
2	7	4.85	0.00	9.23	3	2.99	12.80	106.4	12	4.50	15.00	22.5
3	1	3.33	1.76	39.9	8	4.65	15.00	101.3	3	2.73	22.07	103.9
4	11	4.85	6.00	54.7	1	2.99	2.20	28.3	2	6.27	7.93	6.4
5	4	6.37	10.24	95.8	4	6.31	12.80	98.2	11	4.50	15.00	21.6
6	6	7.00	6.00	12.6	12	4.65	7.50	61.7	5	2.00	15.00	105.4
7	8	4.85	12.00	99.7	13	4.65	7.50	65.4	6	7.00	15.00	16.5
8	12	4.85	6.00	68.3	9	4.65	7.50	68.9	4	6.27	22.07	83.2
9	2	6.37	1.76	6.4	2	6.31	2.20	15.3	7	4.50	5.00	13.3
10	9	4.85	6.00	52.6	11	4.65	7.50	71.3	10	4.50	15.00	28.7
11	10	4.85	6.00	48.3	10	4.65	7.50	76.4	9	4.50	15.00	23.7
12	13	4.85	6.00	50.2	7	4.65	0.00	14.3	1	2.73	7.93	28.2
13	5	2.70	6.00	105.4	5	2.30	7.50	101.2	13	4.50	15.00	37.1

Table 4
Criteria for multiple response optimization with RSM predictions.

Conc. (mg L^{-1})	Prediction									Validation	
	Parameter	Goal	Low. limit	Up. limit	Weight	Importance	pH$_i$	Optimal Cl$^-$ (mM)		CE (%)	RE (%)
104	pH$_i$	Is equal to	3.30	6.34	1	3	3.30	7.9		102.1	6.9
	Cl$^-$	Minimize	0	14	1	3	4.85	10.5		99.3	4.3
	CE	Is in range	95	100	1	3	6.37	13.1		99.8	4.8
260	pH$_i$	Is equal to	2.99	6.31	1	3	2.99	9.8		98.5	3.6
	Cl$^-$	Minimize	0	15	1	3	4.65	12.0		99.2	4.2
	CE	Is in range	95	100	1	3	6.31	14.2		98.7	3.7
520	pH$_i$	Is equal to	2.73	6.27	1	3	2.73	20.0		99.0	3.2
	Cl$^-$	Minimize	5	25	1	3	4.50	24.2		99.5	4.5
	CE	Is in range	95	100	1	3	6.27	24.7		98.4	3.5

Table 5
Comparison of the predicted optimal Cl$^-$ between proposed method and RSM.

Cr(VI)$_i$	104 mg L^{-1}			260 mg L^{-1}			520 mg L^{-1}			RE aver. (%)
pH$_i$	3.30	4.85	6.37	3.0	4.65	6.31	2.73	4.50	6.27	
Our proposed (mM)	6.2	10.2	12.2	10.2	12.5	14.3	19.7	23.0	25.1	1.2 ± 0.8
RSM (mM)	7.9	10.5	13.1	9.8	12.0	14.2	20.0	24.2	24.7	4.3 ± 1.0

showed that all three models were suitable to analyze the factors [38]. The following polynomial equations (Eqs. 3–5) in coded form were determined and evaluated to predict the optimal concentration of Cl$^-$ for depassivation by RSM (Table 4), which matched the results of validation experiments [9,12].

For 104 mg L^{-1}: $y_1 = 57.40 - 21.50x_{11} + 35.07x_{12}$ (3)

For 260 mg L^{-1}: $y_2 = 64.76 - 14.67x_{21} + 35.50x_{22}$ (4)

For 520 mg L^{-1}: $y_3 = 26.72 - 21.03x_{31} + 34.16x_{32} + 16.35x_{31}^2 + 13.88x_{32}^2$ (5)

It is worth noting that the optimal concentration of Cl$^-$ obtained using proposed method is more accurate and stable (lower RE aver. (%)) compared with RSM (Table 5). Therefore, these results verify that the proposed method can be used to effectively optimize the concentration of Cl$^-$ for depassivation during the Fe^0-EC process.

4. Conclusions

Passivation inevitably occurred when pH$_i$ and Cr(VI)$_i$ were in passivation region III or the evolution of pH and Cr(VI) enter passivation region III, even if their initial values were in dissolution region II. The sequence of the resistance of chloride-induced pitting dissolution in these three conditions was pH 8 and Cr(VI) = 520 mg L^{-1} > pH 4 and Cr(VI) = 520 mg L^{-1} > pH 8 and Cr(VI) = 52 mg L^{-1}, which was consistent with the stability of its passive film. MCPD data in passivation region III was determined from galvanostatic measurements. The optimal concentration of Cl$^-$ obtained using our proposed method was more accurate and stable compared with RSM. The proposed method can be used to effectively optimize the concentration of Cl$^-$ for depassivation during the Fe^0-EC process.

References

[1] G. Chen, Electrochemical technologies in wastewater treatment, Sep. Purif. Technol. 38 (2004) 11–41.
[2] X. Chen, G. Chen, Electroflotation, in: C. Comninellis, G. Chen (Eds.), Electrochemistry for the Environment, Springer, New York, 2010, pp. 263–277.

[3] P.K. Holt, G.W. Barton, M. Wark, C.A. Mitchell, A quantitative comparison between chemical dosing and electrocoagulation, Colloids Surf. Physicochem. Eng. Aspects 211 (2002) 233–248.

[4] M.A. Rodrigo, P. Cañizares, C. Buitrón, C. Sáez, Electrochemical technologies for the regeneration of urban wastewaters, Electrochim. Acta 55 (2010) 8160–8164.

[5] P. Xu, G.M. Zeng, D.L. Huang, C.L. Feng, S. Hu, M.H. Zhao, C. Lai, Z. Wei, C. Huang, G.X. Xie, Z.F. Liu, Use of iron oxide nanomaterials in wastewater treatment: a review, Sci. Total Environ. 424 (2012) 1–10.

[6] C. Phalakornkule, P. Sukkasem, C. Mutchimsattha, Hydrogen recovery from the electrocoagulation treatment of dye-containing wastewater, Int. J. Hydrogen Energy 35 (2010) 10934–10943.

[7] E. Ali, Z. Yaakob, Electrocoagulation for Treatment of Industrial Effluents and Hydrogen Production, Edited by Janis Kleperis and Vladimir Linkov (2012) 227.

[8] M.G. Arroyo, V. Perez-Herranz, M.T. Montanes, J. Garcia-Anton, J.L. Guinon, Effect of pH and chloride concentration on the removal of hexavalent chromium in a batch electrocoagulation reactor, J. Hazard. Mater. 169 (2009) 1127–1133.

[9] H.Y. Xu, Z.H. Yang, G.M. Zeng, Y.L. Luo, J. Huang, L.K. Wang, P.P. Song, X. Mo, Investigation of pH evolution with Cr(VI) removal in electrocoagulation process: proposing a real-time control strategy, Chem. Eng. J. 239 (2014) 132–140.

[10] P.p. Song, Z.h. Yang, H.y. Xu, J. Huang, X. Yang, L.k. Wang, Investigation of influencing factors and mechanism of antimony and arsenic removal by electrocoagulation using Fe–Al electrodes, Ind. Eng. Chem. Res. 53 (2014) 12911–12919.

[11] P. Lakshmipathiraj, G.B. Raju, M.R. Basariya, S. Parvathy, S. Prabhakar, Removal of Cr (VI) by electrochemical reduction, Sep. Purif. Technol. 60 (2008) 96–102.

[12] Z.H. Yang, H.Y. Xu, G.M. Zeng, Y.L. Luo, X. Yang, J. Huang, L.K. Wang, P.P. Song, The behavior of dissolution/passivation and the transformation of passive films during electrocoagulation: influences of initial pH, Cr(VI) concentration, and alternating pulsed current, Electrochim. Acta 153 (2015) 149–158.

[13] K.L. Dubrawski, C. Du, M. Mohseni, General potential-current model and validation for electrocoagulation, Electrochim. Acta 129 (2014) 187–195.

[14] P. Holt, G. Barton, C. Mitchell, Electrocoagulation as a wastewater treatment, Third Annu. Aust. Environ. Eng. Res. Event 1000 (1999) 41–46.

[15] E. Keshmirizadeh, S. Yousefi, M.K. Rofouei, An investigation on the new operational parameter effective in Cr(VI) removal efficiency: a study on electrocoagulation by alternating pulse current, J. Hazard. Mater. 190 (2011) 119–124.

[16] A.K. Golder, A.K. Chanda, A.N. Samanta, S. Ray, Removal of hexavalent chromium by electrochemical reduction–precipitation: investigation of process performance and reaction stoichiometry, Sep. Purif. Technol. 76 (2011) 345–350.

[17] K. Dermentzis, A. Christoforidis, E. Valsamidou, A. Lazaridou, N. Kokkinos, Removal of hexavalent chromium from electroplating wastewater by electrocoagulation with iron electrodes, Glob. Nest J. 13 (2011) 412–418.

[18] G. Mouedhen, M. Feki, M. De Petris-Wery, H.F. Ayedi, Electrochemical removal of Cr(VI) from aqueous media using iron and aluminum as electrode materials: towards a better understanding of the involved phenomena, J. Hazard. Mater. 168 (2009) 983–991.

[19] T. Olmez, The optimization of Cr(VI) reduction and removal by electrocoagulation using response surface methodology, J. Hazard. Mater. 162 (2009) 1371–1378.

[20] S. Aber, A.R. Amani-Ghadim, V. Mirzajani, Removal of Cr(VI) from polluted solutions by electrocoagulation: modeling of experimental results using artificial neural network, J. Hazard. Mater. 171 (2009) 484–490.

[21] T. Tsuru, S.-I. Nakao, S. Kimura, Ion separation by bipolar membranes in reverse osmosis, J. Membr. Sci. 108 (1995) 269–278.

[22] C. Noubactep, A. Schöner, Metallic iron for environmental remediation: learning from electrocoagulation, J. Hazard. Mater. 175 (2010) 1075–1080.

[23] H. Sarahney, X. Mao, A.N. Alshawabkeh, The role of iron anode oxidation on transformation of chromium by electrolysis, Electrochim. Acta 86 (2012) 96–101.

[24] H.Y. Ha, H.S. Kwon, Effects of pH levels on the surface charge and pitting corrosion resistance of Fe, J. Electrochem. Soc. 159 (2012) C416–C421.

[25] S. Liu, H. Sun, L. Sun, H. Fan, Effects of pH and Cl⁻ concentration on corrosion behavior of the galvanized steel in simulated rust layer solution, Corros. Sci. 65 (2012) 520–527.

[26] M. Saremi, E. Mahallati, A study on chloride-induced depassivation of mild steel in simulated concrete pore solution, Cem. Concr. Res. 32 (2002) 1915–1921.

[27] M.B. Valcarce, M. Vazquez, Carbon steel passivity examined in solutions with a low degree of carbonation: the effect of chloride and nitrite ions, Mater. Chem. Phys. 115 (2009) 313–321.

[28] S.A.M. Refaey, Inhibition of steel pitting corrosion in HCl by some inorganic anions, Appl. Surf. Sci. 240 (2005) 396–404.

[29] Y.F. Cheng, J.L. Luo, Passivity and pitting of carbon steel in chromate solutions, Electrochim. Acta 44 (1999) 4795–4804.

[30] W.P. Yang, D. Costa, P. Marcus, Resistance to pitting and chemical composition of passive films of a Fe–17%Cr alloy in chloride-containing acid solution, J. Electrochem. Soc. 141 (1994) 2669–2676.

[31] A. Kocijan, C. Donik, M. Jenko, Electrochemical and XPS studies of the passive film formed on stainless steels in borate buffer and chloride solutions, Corros. Sci. 49 (2007) 2083–2098.

[32] A.D. Eaton, L.S. Clesceri, A.E. Greenberg, M.A.H. Franson, A.P.H. Association, A. W.W. Association, W.E. Federation, Standard Methods for the Examination of Water and Wastewater, American Public Health Association, 1998.

[33] H. Deng, H. Nanjo, P. Qian, A. Santosa, I. Ishikawa, Y. Kurata, Potential dependence of surface crystal structure of iron passive films in borate buffer solution, Electrochim. Acta 52 (2007) 4272–4277.

[34] R.-H. Jung, H. Tsuchiya, S. Fujimoto, XPS characterization of passive films formed on Type 304 stainless steel in humid atmosphere, Corros. Sci. 58 (2012) 62–68.

[35] Y.F. Cheng, J.L. Luo, A comparison of the pitting susceptibility and semiconducting properties of the passive films on carbon steel in chromate and bicarbonate solutions, Appl. Surf. Sci. 167 (2000) 113–121.

[36] S. Ahn, H. Kwon, Diffusivity of point defects in the passive film on Fe, J. Electroanal. Chem. 579 (2005) 311–319.

[37] A. Dhanapal, S. Rajendraboopathy, V. Balasubramanian, S.R. Rao, A.R.T. Zaman, Effect of pH values, chloride ion concentration and exposure time on pitting corrosion rates of friction stir welded AZ61A magnesium alloy in sodium chloride solution using surface response methodology, Corros. Eng. Sci. Technol. 47 (2012) 425–440.

[38] J. Huang, Z.H. Yang, G.M. Zeng, M. Ruan, H.Y. Xu, W.C. Gao, Y.L. Luo, H.M. Xie, Influence of composite flocculant of PAC and MBFGA1 on residual aluminum species distribution, Chem. Eng. J. 191 (2012) 269–277.